Supporting Information

Interfacial Adsorption-Enabled Trace Additives for Stable Zinc-Based Flow Batteries

Ziyi Huang[1,2#,] Xi Chen[1,2#], Zhaoxia Hou[1,2], Yunxuan Li[2], Xinyue Liu[2], Jianyang Wu[3], Mingyue Zhou[2*], Wen Liu[1*]

1. State Key Laboratory of Chemical Resource Engineering, College of Chemistry, Beijing University of Chemical Technology, Beijing, 100092, China
2. College of Carbon Neutrality Future Technology, China University of Petroleum-Beijing, Beijing, 102200, China
3. College of Chemistry and Molecular Engineering, Peking University, 100871 Beijing, China

Corresponding Author

* E-mail: mingyue.zhou@cup.edu.cn (M. Zhou)

* E-mail: wenliu@mail.buct.edu.cn (W. Liu).

Experience Section

1.1 Material

Zinc oxide, sodium hydroxide, potassium ferrocyanide, potassium ferricyanide, and sodium chloride were bought from Aladdin-Holdings Group. 3-[bis (2-hydroxyethyl) amino]-2-hydroxy-propane sulphonic acid was bought from Shanghai Macklin Biochemical Co., Ltd. The Nafion 117 and Nafion 212 were bought from 3Achem. These reagents were of analytical grade. The graphite felts were bought from Liaoyang J-Carbon Materials Co., Ltd., China. The single cell is manufactured by Wuhan Zhisheng New energy Co., Ltd.

1.2 Characterizations

The morphologies of the zinc metal deposited on the graphite felt were characterized by scanning electron microscopy (SEM, ISM-7500E, Japan). The elemental composition of the samples was determined using energy dispersive spectroscopy (EDS) by the ISM-7500E, Japan. Raman spectra of different electrolytes were recorded using high-resolution Raman (Lab-RAM HR Evolution). At 532 nm to reveal the solvation structural evolution of blank electrolyte. The absorption of DIPSO on the zinc plate was verified by the Fourier transform infrared (FTIR, FTIR-650, China) spectrometer at a scan rate of 32 with a resolution of $4cm^{-1}$. Moreover, to confirm the absorption between DIPSO and deposited Zn layer, X-ray

photoelectron spectroscopy (XPS) (Thermo Scientific K-Alpha, USA) was measured.

Cyclic voltammetry (CV), linear sweep voltammetry (LSV), and chronoamperometry (CA) tests were performed on a conventional three-electrode system in a solution of 0.2 M $Zn(OH)_4^{2-}$ with and without 0.01 M DIPSO. Cyclic voltammetry (CV) was performed on a CS2350M electrochemical workstation, which employs a three-electrode system with a glass carbon as the working electrode, Hg/HgO as the reference electrode, and a graphite plate as the counter electrode. The diameter of glass carbon is 3 mm, and it was polished by alumina slurry for several minutes and then washed with deionized water before testing. Tafel curves were also conducted based on a three-electrode system using a zinc plate (1 cm^2) as the working electrode, Hg/HgO as the reference electrode, and a graphite plate as the counter electrode.

1.3 Battery performances

In an alkaline zinc-iron flow battery, graphite felts were used as both cathode and anode, and N117 was used to separate the catholyte and anolyte. The ion exchange membrane undergoes pretreatment with hydrogen peroxide and sulfuric acid before use. The current density and areal capacity were calculated using the specific area of graphite felt in this work. To make sure the capacity is limited by the anode and the SOC can

be calculated based on the discharged capacity and theoretical capacity of zincate ions, the capacity of catholyte is excessive. For zinc-iron flow batteries (ZIFBs) with an areal capacity of 30 mAh cm^{-2} at 80 mA cm^{-2}, the specific area of graphite felt was 4 cm^2, 15 mL 0.2 M $Zn(OH)_4^{2-}$/3 M NaOH was used as anolyte, and 100 mL 1 M NaCl/0.4 M $K_4Fe(CN)_6$/0.05 M $K_3Fe(CN)_6$ was used as catholyte. For zinc-iron flow battery with an areal capacity of 80 mAh cm^{-2} at 80 mA cm^{-2}, the specific area of graphite felt was 10.89 cm^2, 135 mL 0.2 M $Zn(OH)_4^{2-}$/3 M NaOH was used as anolyte, and 500 mL 1 M NaCl/0.4 M $K_4Fe(CN)_6$/0.05 M $K_3Fe(CN)_6$ was used as catholyte.

The Zn||Zn symmetrical flow battery was assembled by using zinc metal (0.02 cm) sandwiched in graphite felt as cathode and anode. 60 mL of 0.2 M $Zn(OH)_4^{2-}$/3 M NaOH with or without DIPSO was used as catholyte and anolyte. The test was carried out by stripping and plating a given amount of Zn metal.

1.4 Calculation

1.4.1 Molecular dynamics (MD) simulation and density function theory (DFT) calculations

To analyze the solvation structure and interaction between DIPSO and deposited Zn, MD simulation and DFT calculations were performed. In the MD simulation, All the calculations were performed with the Forcite software package. The Universal Forcefield (UFF)[1] was used as the energy expression of phase energy surface (PES). The Qeq method[2] was applied

to assign the atomic charge with the tolerance of 5×10^{-4} e. The non-bond interaction was evaluated by the Ewald method[3] with the Ewald accuracy of 10^{-5} kcal/mol. During the optimization process, all the atoms were allowed to relax. The convergence criteria for energy change are 2×10^{-5} kcal/mol and for force is 0.001 kcal/mol/Å. After the geometry optimization, a 100 ps of NVT molecular dynamics (MD) simulation was performed and then followed by 150 ps of NPT simulations with the time step of 1 fs. The data was collected in the production phase for 1 ns. The Andersen method[4] was used to maintain the temperature and the Berendsen method[5] was applied to control the pressure during the simulation.

All spin-polarized density-functional theory (DFT) computations were performed using the Vienna ab initio simulation package (VASP)[6] based on the projector augmented wave (PAW)[7] method. Electron-ion interactions were described using standard PAW potentials. A plane-wave basis set was employed to expand the smooth part of the wave functions with a cutoff kinetic energy of 400 eV. For the Electron-electron exchange and correlation interactions, the functional parametrized by Perdew-Burke-Ernzerhof (PBE)[8], a form of the general gradient approximation (GGA), was used throughout. The Van der Waals interaction was described via the DFT-D3BJ method[9]. To study the mechanistic chemistry of surface reactions, the surface was modeled with a slab model. A sufficiently large vacuum region of 15 Å was used to ensure the periodic images were well

separated. During the geometry optimizations, the bottom atoms were fixed at the bulk position when the surface properties were calculated. In this work, the Brillouin-zone integrations were conducted using Monkhorst-Pack grids[10] of special points with a separation of 0.05 $Å^{-1}$. The convergence criterion for the electronic self-consistent loop was set to 10^{-5} eV. The atomic structures were optimized until the residual forces were below 0.05 eV $Å^{-1}$.

1.4.2 Cost calculation

The cost of DIPSO chemicals is referred to the website (detail.1688.com), marginal cost of the battery can be estimated according to the following equations:

$$Cost\ of\ DIPSO = \frac{P \times m}{Q_a \times V_{cell}} = \frac{1.2356 \times 0.0365}{0.16 \times 1.74} = 0.162\ \$/kWh$$

where subscript a represents anolyte, P is the price of additive (\$ Kg^{-1}), m is the quality of additives used in anolyte (g), Q_a is the capacity of the anode (Ah), and V_{cell} is the voltage of alkaline zinc-iron flow battery.

1.4.3 Power density calculation

The power density can be calculated according to the equation: $P = \frac{I \times V_{cell}}{A} (mW\ cm^{-2})$[11]

Supplementary Figures

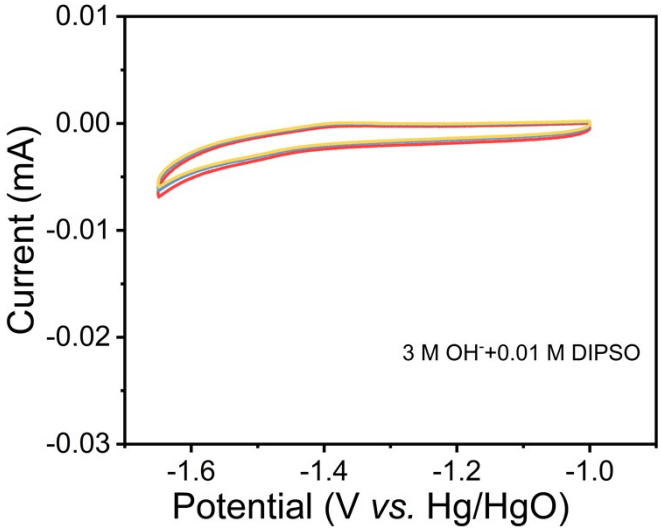

Fig. S1 The CV of 0.01 M DIPSO in 3 M NaOH solution at the scan rate of 30 mV s^{-1}

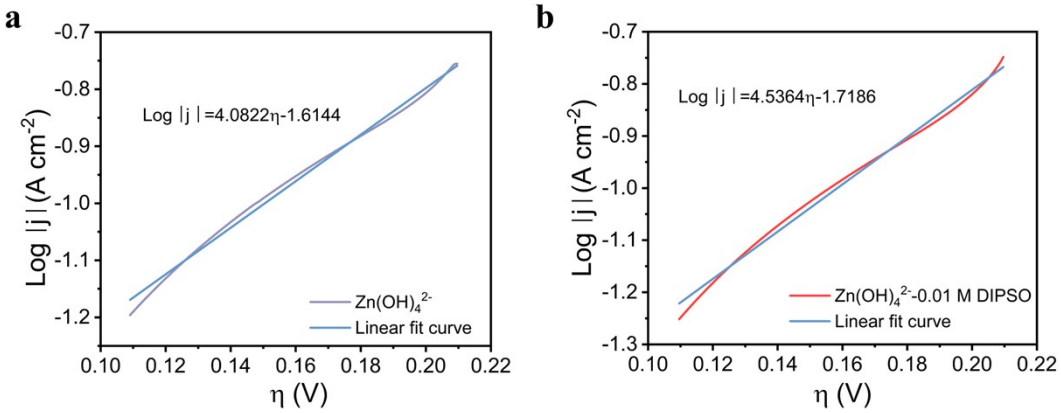

Fig. S2 The linear fit curve of log |j| *vs.* overpotential

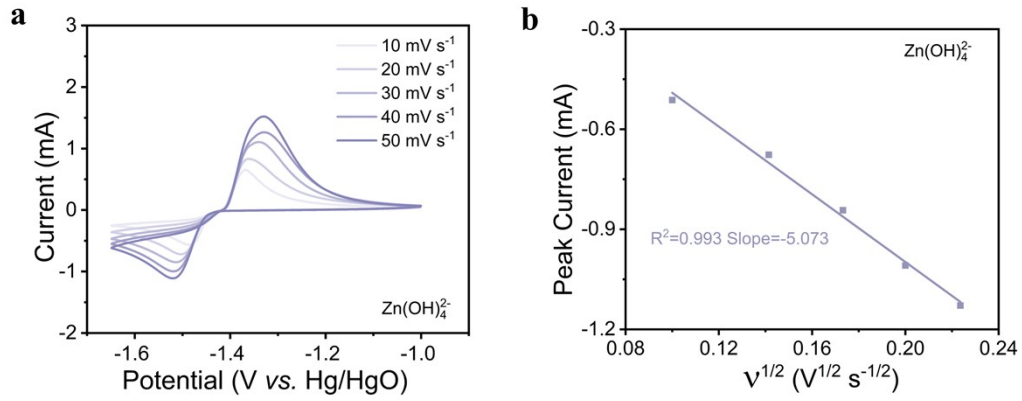

Fig. S3 (a) Cyclic voltammetry test of blank electrolyte at different scan rates. (b) Peak current *vs*. the square root of scan rate

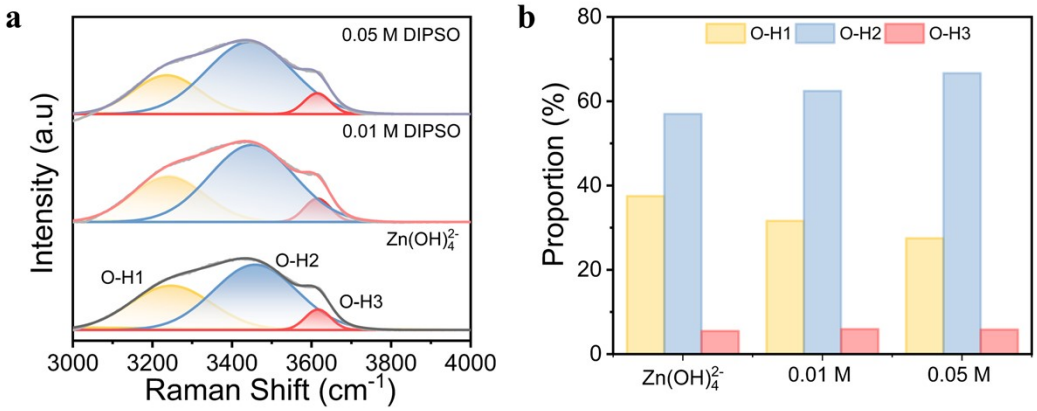

Figure S4. (a) Raman spectra of various electrolytes at the wavenumber range of O-H stretching vibration. (b) correlations of H-bonds ratio

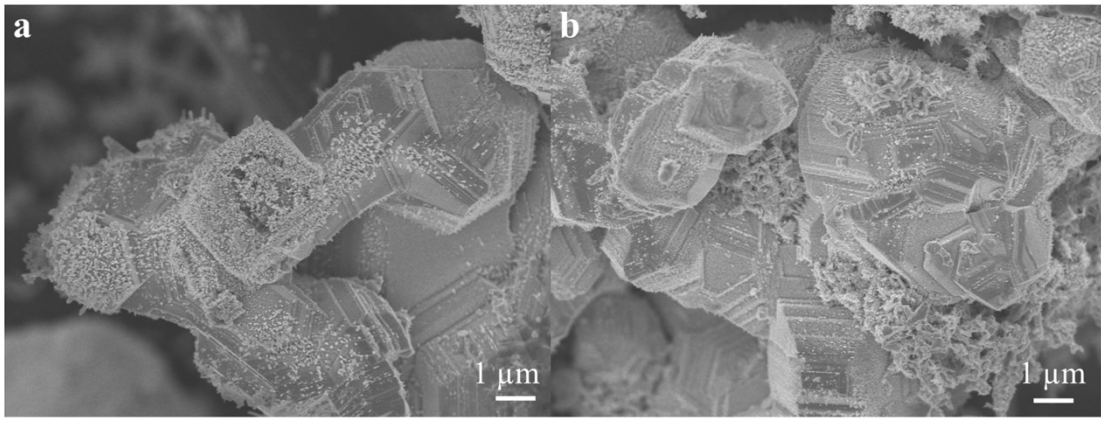

Fig. S5 0.05 M DIPSO-added electrolyte in ZIFBs at the end of charging

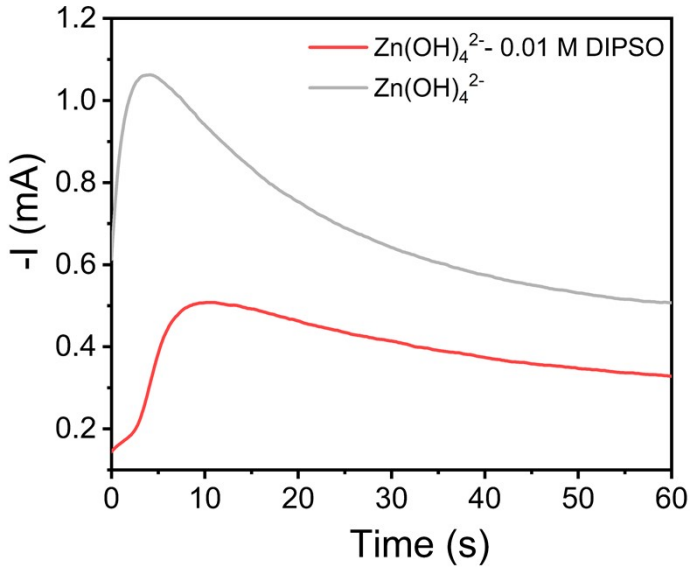

Fig. S6 Chronoamperograms measured at -1.46 V in 0.2 M $Zn(OH)_4^{2-}$ and 0.01 M DIPSO-added electrolytes, respectively.

Theoretically, instantaneous nucleation means that all nuclei appear simultaneously at all possible growth sites on the initial barrier step and then grow at the same rate; the nucleation sites are gradually activated in a progressive nucleation mode, and the nucleation process is accompanied by the growth of the nucleus. Instantaneous nucleation and progressive nucleation are expressed as follows:

Instantaneous:

$$(j/j_m)^2 = 1.9542\,(t/t_m)^{-1}\left\{1 - exp\left[-1.2564\left(\frac{t}{t_m}\right)\right]\right\}^2 \quad (1)$$

Progressive:

$$(j/j_m)^2 = 1.2254\,(t/t_m)^{-1}\left\{1 - exp\left[-2.3367\left(\frac{t}{t_m}\right)^2\right]\right\}^2 \quad (2)$$

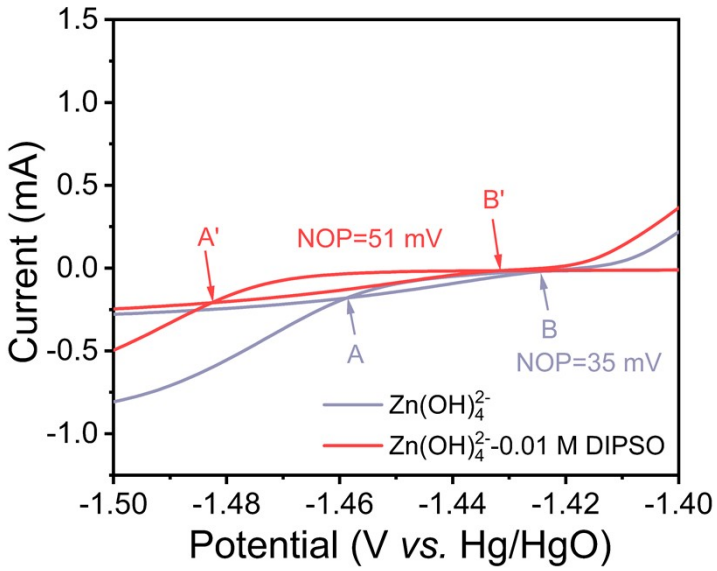

Fig. S7 Cyclic voltammograms of Blank and DIPSO-added electrolyte

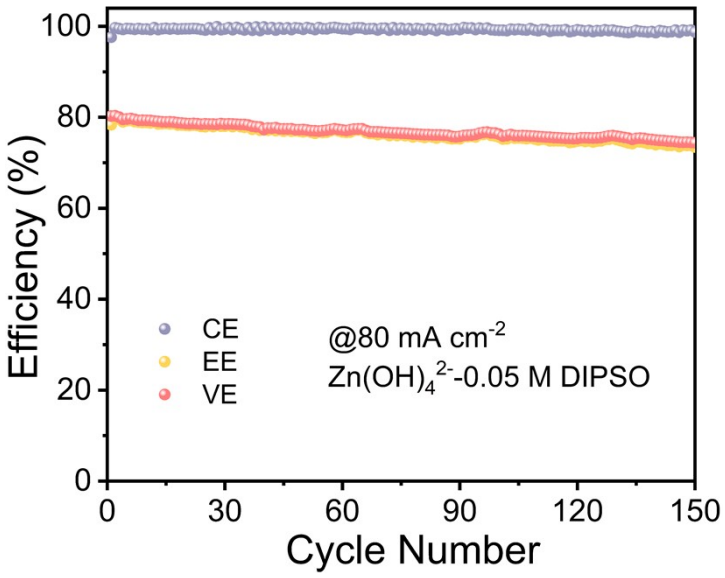

Fig. S8 The cycling stability of ZIFB using anolyte with 0.05 M DIPSO

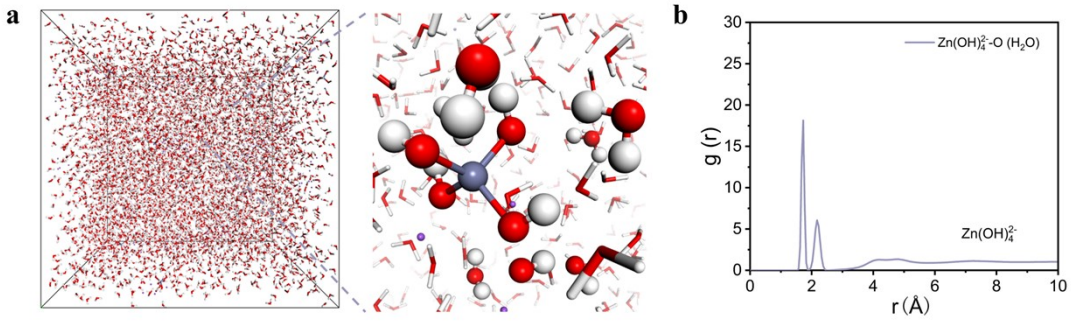

Fig. S9 (a) 3D snapshot from MD simulations representing the solvation structure of $Zn(OH)_4^{2-}$. (b) Radial distribution function for $Zn(OH)_4^{2-}$

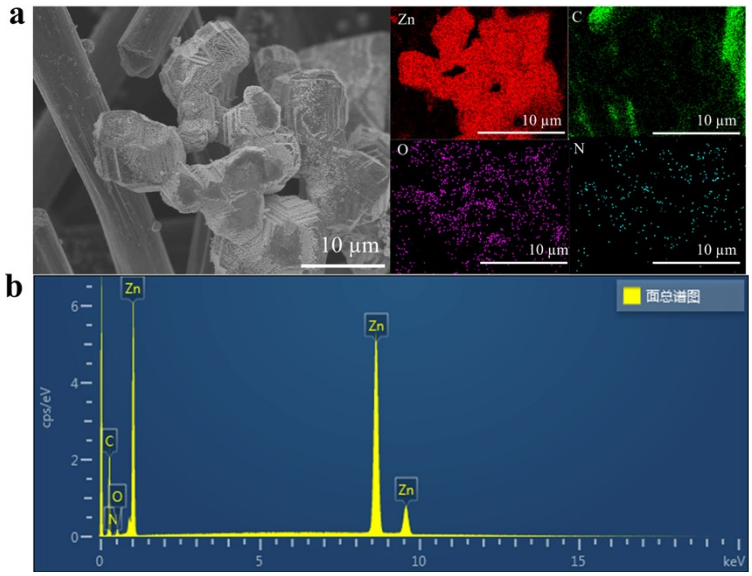

Fig.S10 Morphology of zinc-plated carbon felt in DIPSO and corresponding energy dispersive X-ray analysis elemental maps of Zn, O, C, and N

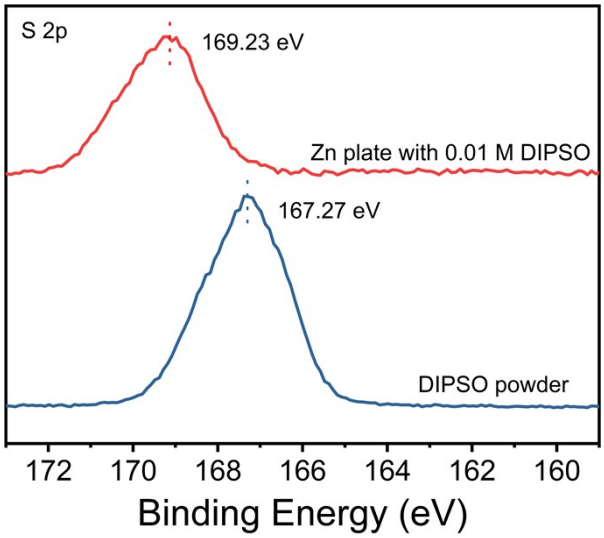

Fig. S11 S 2p XPS spectrum of DIPSO powder and Zn after immersion in electrolyte with DIPSO for 5 days

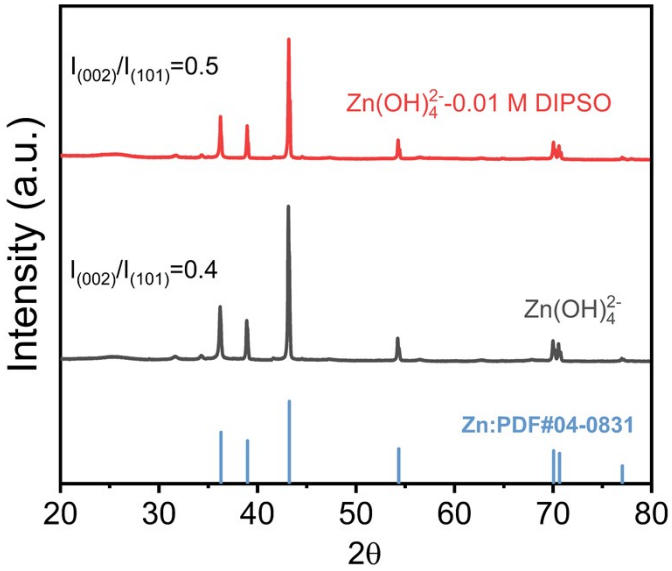

Fig. S12 XRD pattern of deposited zinc on the carbon felt at 20 mAh cm^{-2} and 80 mA cm^{-2}

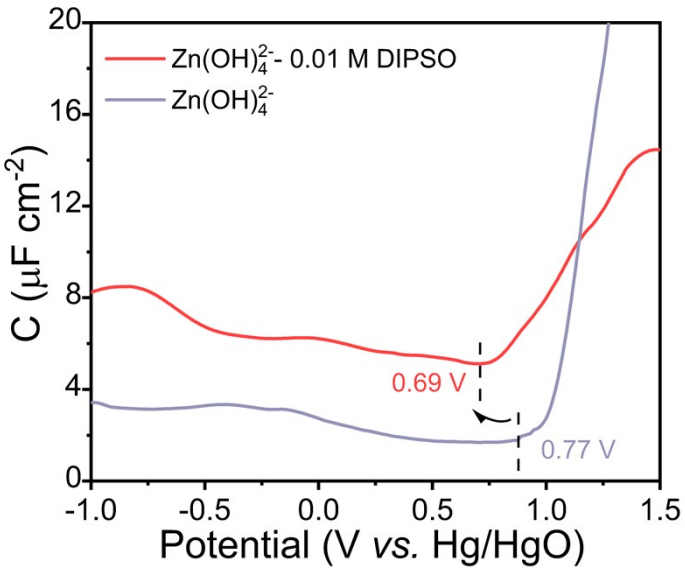

Fig. S13 The differential capacitance-potential curves for electrodes in blank and DIPSO-added electrolytes.

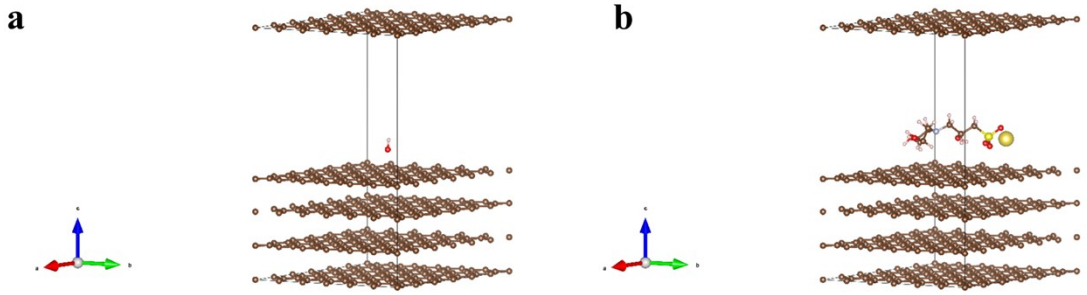

Fig. S14 DFT calculated the adsorption structures of OH^- and DIPSO on the graphite surface respectively

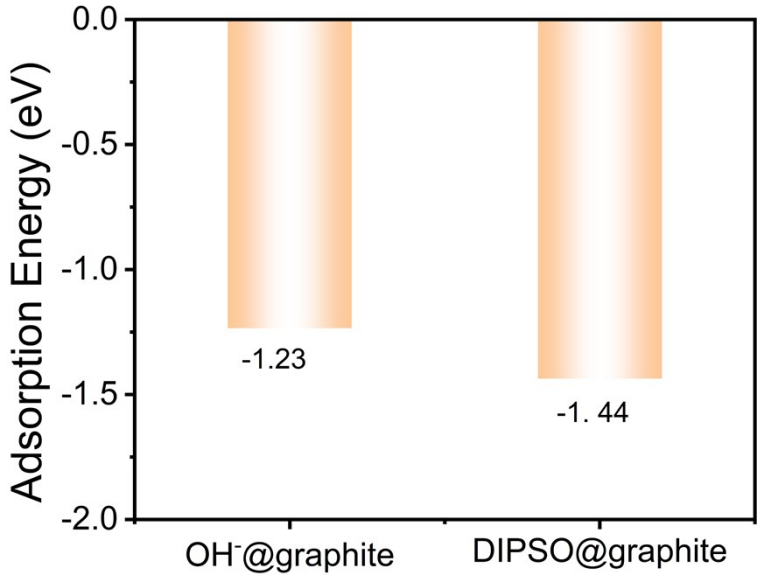

Fig. S15 The comparison of adsorption energies on the graphite

Table S1. The comparison of performance with other zinc-iron flow batteries

Electrolyte	Current Density	CE	Cycling stability	SOC (zinc anode)	reference
$Zn(OH)_4^{2-}$+DIPSO	80 mA cm^{-2}	99.5%	300 cycles (225h)	75%	This work
$Zn(OH)_4^{2-}$+THEED	80 mA cm^{-2}	~99.8%	~180 cycles (120h)	70%	[12]
$Zn(OH)_4^{2-}$+urea	50 mA cm^{-2}	98.5%	130 h	~60%	[13]
$Zn(OH)_4^{2-}$+PEG	80 mA cm^{-2}	98.53%	120 cycles (192 h)	37.3%	[14]
$Zn(OH)_4^{2-}$+EDTA	80 mA cm^{-2}	99.6%	>300 h	70%	[15]
$ZnBr_2$+EG+KGlu	20 mA cm^{-2}	97.4%	200 cycles	~45%	[16]
$ZnCl_2$+NAM	20 mA cm^{-2}	-	120 h	~34.8%	[17]
$ZnCl_2$+$CaCl_2$+NH_4Cl	20 mA cm^{-2}	94%	>40 cycles		[18]
$ZnAc_2$+Cit	40 mA cm^{-2}	99.8%	400 cycles	50%	[19]

Reference

1 A. K. Rappe, C. J. Casewit, K. S. Colwell, W. A. Goddard and W. M. Skiff, *J. Am. Chem. Soc.*, 1992, **114**, 10024–10035.

2 A. K. Rappe and W. A. Goddard, *J. Phys. Chem.*, 1991, **95**, 3358–3363.

3 N. Karasawa and W. A. Goddard, *J. Phys. Chem.*, 1989, **93**, 7320–7327.

4 H. C. Andersen, *The Journal of Chemical Physics*, 1980, **72**, 2384–2393.

5 H. J. C. Berendsen, J. P. M. Postma, W. F. Van Gunsteren, A. DiNola and J. R. Haak, *The Journal of Chemical Physics*, 1984, **81**, 3684–3690.

6 J. Hafner, *Journal of Computational Chemistry*, 2008, **29**, 2044–2078.

7 P. E. Blöchl, *Phys. Rev. B*, 1994, **50**, 17953–17979.

8 J. P. Perdew, K. Burke and M. Ernzerhof, *Phys. Rev. Lett.*, 1996, **77**, 3865–3868.

9 S. Grimme, S. Ehrlich and L. Goerigk, *Journal of Computational Chemistry*, 2011, **32**, 1456–1465.

10 H. J. Monkhorst and J. D. Pack, *Phys. Rev. B*, 1976, **13**, 5188–5192.

11 Y. Yao, J. Lei, Y. Shi, F. Ai and Y.-C. Lu, *Nat Energy*, 2021, **6**, 582–588.

12 L. Zhi, T. Li, X. Liu, Z. Yuan and X. Li, *Nano Energy*, 2022, **102**, 107697.

13 R. Ling, Z. Zhu, K. Peng, J. Fang, W. Zou, Q. Li, Y. Liu, Q. Zhu, N. Lin, T. Xu and Z. Yang, *Advanced Materials*, **n/a**, 2404834.

14 D. Chen, C. Kang, W. Duan, Z. Yuan and X. Li, *Journal of Membrane Science*, 2021, **618**, 118585.

15 L. Zhi, C. Liao, P. Xu, F. Sun, C. Yuan, F. Fan, G. Li, Z. Yuan and X. Li, *Energy Environ. Sci.*, DOI:10.1039/D3EE02693K.

16 T. Xuan, X. Cheng and L. Wang, *Journal of Power Sources*, 2024, **614**, 234975.

17 J. Yang, H. Yan, H. Hao, Y. Song, Y. Li, Q. Liu and A. Tang, *ACS Energy Lett.*, 2022, **7**, 2331–2339.

18 Y. Zhang, D. Henkensmeier, S. Kim, R. Hempelmann and R. Chen, *Journal of Energy Storage*, 2019, **25**, 100883.

19 Z. Chen, T. Li, C. Xie and X. Li, *ACS Energy Lett.*, 2024, 3426–3432.